



## Evaluating the impact of atmospheric forcing resolution and air-sea coupling on near-coastal regional ocean prediction

Huw W. Lewis<sup>1</sup>, John Siddorn<sup>1</sup>, Juan Manuel Castillo Sanchez<sup>1</sup>, Jon Petch<sup>1</sup>, John M. Edwards<sup>1</sup>, Tim Smyth<sup>2</sup>

5

<sup>1</sup>Met Office, Exeter, EX1 3PB, UK

<sup>2</sup>Plymouth Marine Laboratory, Plymouth, PL1 3DH, UK

*Correspondence to:* Huw W. Lewis ([huw.lewis@metoffice.gov.uk](mailto:huw.lewis@metoffice.gov.uk))

### Abstract.

- 10 Atmospheric forcing applied as ocean model boundary conditions can have a critical impact on the quality of ocean forecasts. This paper assesses the sensitivity of an eddy-resolving (1.5 km resolution) regional ocean model of the North-West European shelf (NWS) to atmospheric forcing resolution and air-sea coupling. The analysis is focused on a month-long simulation experiment for July 2014 and evaluation of simulated sea surface temperature (SST) in a shallow near-coastal region to the south-west of the UK (Celtic Sea and western English Channel). Observations above and below the sea surface at the L4 ocean
- 15 buoy from the Western Channel Observatory are used to evaluate ocean and atmosphere model data. The impacts of differences in the atmospheric forcing are illustrated by comparing results from an ocean model run in forcing mode using operational global-scale numerical weather prediction (NWP) data with a run forced by a convective scale regional atmosphere model. The value of dynamically representing feedbacks between the atmosphere and ocean state is assessed through use of these model components within a fully coupled ocean-wave-atmosphere system.
- 20 Simulated SST show considerable sensitivity to atmospheric forcing and to the impact of model coupling in near-coastal areas. A warm ocean bias relative to in-situ observations in the simulation forced by global-scale NWP (0.7 K mean difference, warmer relative to all observations in the model domain) is shown to be reduced (to 0.4 K) through use of the 1.5 km resolution atmosphere forcing. When simulated in coupled mode, this bias is further reduced by 0.2 K. Results demonstrate much greater variability of both surface energy balance terms and near-surface winds in the higher
- 25 resolution atmosphere model data, as might be expected. Assessment of the surface energy balance and wind forcing over the ocean is challenging due to a scarcity of observations. It can however be demonstrated that the wind speed over the ocean simulated by the high resolution atmosphere agreed with the limited number of observations less well than the global-scale NWP data. Further partially-coupled experiments are discussed to better understand why the degraded wind forcing does not detrimentally impact on SST results.



## 1 Introduction

The exchanges of heat and momentum across the air-sea interface are fundamental components of the climate system (e.g. Yu et al., 2012), and can play a significant role in the evolution of natural hazards (e.g. Wada et al., 2018). In oceanography, accurate representation of the surface energy budget and near-surface winds and momentum fluxes are essential boundary conditions for ocean models given that they drive the ocean energy and dynamics from the surface (e.g. Lellouche et al., 2018). Despite this, routine evaluation of the quality of the surface forcing of operational ocean forecast systems receives relatively little focus. To a large extent, this reflects the challenge of observing these quantities over the ocean compared with on land, and thereby limited availability of measurements for evaluation (Drechsel et al., 2012; Banta et al., 2018). This may also be a result of operational ocean forecast systems running in a ‘forced-mode’ approach, whereby the surface forcing is provided from an external source of atmosphere model data. Typically the evaluation of atmosphere forecast quality is separated, potentially in science and organisational scope, from research and development of ocean forecast systems. Evaluation of wind forcing for operational wave models has been more prevalent, given the strong sensitivity of wave predictions to their accuracy (Cavaleri et al. 2009).

The development of fully coupled atmosphere-ocean modelling prediction systems provide both motivation and tools with which to better understand the impact of the surface forcing on ocean forecasts (e.g. Pullen et al., 2017). This paper discusses an application of a regional coupled system for a North-West European shelf (NWS) domain to assess the impact of atmospheric forcing resolution and air-sea feedbacks on the quality of ocean predictions. The study focusses on a near-coastal region given that it is both where populations and critical infrastructure are located and as they represent complex environments where providing accurate ocean predictions can be more challenging through the strong influence of land-sea contrasts on both atmospheric forcing and ocean models (e.g. Holt et al., 2017; Cavaleri et al., 2018).

An evaluation of the influence of surface fluxes on regional ocean simulations of the Mediterranean Sea was assessed by Lebeaupin Brossier et al. (2011), who found that improving the temporal resolution of the atmospheric forcing, as well as the spatial resolution over some coastal areas, significantly changed the variability of mesoscale ocean processes. Schaeffer et al. (2011) demonstrated improved representation of ocean eddies in the Gulf of Lion with a change from 9 km to 2.5 km resolution wind forcing, but little impact of temporal resolution. Of relevance to the NWS, Bricheno et al. (2012) found a reduction on wind speed errors of more than 10% when moving from use of a 12 km to 4 km resolution atmosphere forcing for a wave-ocean coupled system of the Irish Sea.

A number of studies using a range of regional coupled systems have reported that simulated atmospheric fluxes can be improved through representing air-sea interactions (Lewis et al., 2018a). For example, Carniel et al. (2016) and Licer et al. (2016) assessed the impact of coupling on components of the surface energy budget for different coupled simulations of the Adriatic Sea, and showed that much improved turbulent heat fluxes resulted in improved predictions of sea surface temperature (SST) relative to forced mode ocean simulations. Similar sensitivity was demonstrated by Bruneau and Toumi (2016) for the Caspian Sea. Gronholz et al. (2017) showed improved SST prediction for the North Sea through use of a higher resolution



regional atmosphere forcing rather than a global-scale analysis, and further improvement through coupling between atmosphere and ocean. The influence of improved wind forcing through wave-atmosphere coupling was demonstrated by Wahl et al. (2017) for a similar domain.

The implications of atmospheric forcing resolution and air-sea coupling on ocean forecasts for the NWS are assessed in this paper using the UKC3 regional coupled system. Lewis et al. (2018b) described the system in detail and provided an initial domain-wide assessment of the UKC3 ocean performance for month-long simulations in four different seasons. This study focuses on near-coastal results for one of those periods in July 2014. The application of UKC3 in the current study is described in Sect. 2. Simulated SST and atmosphere forcing are compared with in-situ measurements in Sect. 3 and conclusions drawn in Sect. 4.

## 10 2 Methods

### 2.1 Ocean model configurations and atmospheric forcing

This study makes use of the AMM15 (Atlantic Margin Model, 1.5 km horizontal grid resolution) ocean model configuration, as described in detail by Graham et al. (2018), and in use for operational oceanography across the North-West European shelf (NWS) within the Copernicus Marine Environment Monitoring Service (CMEMS; Tonani et al., 2018, *this issue*). AMM15 uses the NEMO ocean model code (vn3.6\_STABLE, r6232; Madec et al., 2016). The model domain is illustrated in Fig. 1(a), showing the relatively shallow North-West European shelf and shelf-break bounding to the North Atlantic to the west. The forced mode and coupled implementations evaluated in this paper were documented in detail by Lewis et al. (2018b).

A number of forced and coupled simulations spanning a month-long period between 30 June and 31 July 2014 have been conducted. To highlight ocean model performance in a near-coastal environment, the subsequent analysis focusses on evaluation relative to in-situ observations over the ocean within a section of the model domain encompassing the Celtic Sea and surrounding south-western approaches to the UK (Fig. 1(b)). The on-shelf part of this region has water depths of order 50 to 100 m and is seasonally stratified from late-April until September and well mixed through the rest of the year.

A summary of the four simulation experiments considered is given in Table 1. All ocean simulations were initialised from the same initial condition, taken from the 30-year free-running AMM15 simulation documented by Graham et al. (2018). As described by Lewis et al. (2018b), the same lateral boundary conditions using ocean model output from the coupled GloSea5 seasonal prediction system at 1/4° horizontal resolution (MacLachlan et al., 2015) were applied in all simulations. The same climatological freshwater discharge data were also applied to all simulations (Graham et al., 2018).

Experiments FOR\_GL and FOR\_HI are forced mode ocean model simulations, in which externally generated meteorological data were applied via file input. This is the approach most typically used in operational ocean forecast systems (e.g. Tonani et al., 2018, *this issue*). In this study, variables describing the surface energy budget and near-surface wind computed on an external atmosphere model grid are applied as a surface boundary condition in NEMO using the ‘flux formulation’ methodology (Madec et al., 2016). The FOR\_GL and FOR\_HI runs contrast in the spatial and temporal resolution of



meteorological information applied. In FOR\_GL forcing data originating from a global-scale operational weather forecast using the Met Office Unified Model (MetUM) are interpolated onto the 1.5 km resolution ocean grid. For the period considered in this paper, the global MetUM forecast system used the Global Atmosphere (GA) and Global Land (GL) version 6.1 science configurations, documented in detail by Walters et al. (2017a). Across the NWS, global data from this system were available at a horizontal spatial resolution of about 17 km, with radiation variables applied at 3 hourly and wind components at hourly intervals through the simulation. The ocean surface boundary condition in the global MetUM is provided by the daily OSTIA (Operational Sea Surface Temperature and Sea Ice Analysis; Donlon et al., 2012). Surface currents are assumed zero and a constant global value for the wave-dependent roughness Charnock parameter of 0.085 is used.

By contrast, FOR\_HI is forced by variables interpolated from a regional atmosphere configuration of the MetUM, equivalent to that used for regional-scale operational weather prediction at the Met Office (RA1; Bush et al., 2018). The regional atmosphere configuration has a variable resolution grid (Tang et al., 2013), with a region of regularly spaced cells across the UK at 1.5 km horizontal spacing (Fig. 1(a)), and stretching out to 1.5 km x 4 km cells towards the domain boundaries. At this atmosphere model resolution convection is explicitly resolved and local details such as the model coastlines and orography impact on the meteorology (e.g. Clark et al., 2016). All meteorological data from the high resolution system were applied to the ocean at hourly frequency. For the month-long atmosphere simulation considered here, the surface boundary condition to the atmosphere simulation was also provided by interpolation from the daily OSTIA, and kept constant for each 24 h period. As in the global NWP system, ocean surface currents are assumed zero and but a constant value for the Charnock parameter of 0.011 is now assumed. Details of the RA1 regional MetUM configuration, and how they relate to the global-scale NWP configuration, are provided by Bush et al. (2018). One of the key differences, related to the horizontal grid resolution is that atmospheric convection is explicitly represented in FOR\_HI, whereas its simulation is parameterised in FOR\_GL. The treatment of solar and terrestrial radiation also differ between RA1 and GA6.1 configurations. The RA1 configuration is most analogous to that used in GA7, which has an improved treatment of gaseous absorption compared to GA6 which typically result in reduced clear-sky outgoing long-wave radiation and increased downwards surface flux (Walters et al., 2017b). A final key difference between the global and regional MetUM configurations is that the parameterisation of clouds in FOR\_GL uses the PC2 prognostic scheme (Wilson et al., 2008) and in FOR\_HI uses the Smith (1990) diagnostic cloud scheme. One advantage of the prognostic approach is that clouds can be advected away from where they were created, but the diagnostic scheme is still considered to provide better forecasts in mid-latitude regional atmosphere configurations (Bush et al., 2018). Coupled experiments CPL\_AO and CPL\_AOW use the AMM15 ocean model configuration as part of the UKC3 dynamically coupled system (Lewis et al., 2018b). The MetUM atmosphere model component is the same as used in atmosphere-only mode to provide FOR\_HI forcing (i.e. 1.5 km variable resolution grid and RA1 science configuration), but now coupled directly to the ocean using the OASIS3-MCT (Valcke et al., 2015) libraries with all information exchanged at hourly frequency. The CPL\_AO simulation involves only atmosphere and ocean components being coupled. The ‘fully coupled’ CPL\_AOW simulation also incorporates coupling between both atmosphere and ocean models to the WAVEWATCH III (Tolman et al., 2004) spectral wave model, defined on the same model grid as AMM15.



## 2.2 In-situ observations and the Western Channel Observatory

Atmosphere and ocean model simulations from these experiments are compared to in-situ observations obtained from the operational network of surface automatic weather stations, ships and drifting or moored ocean buoys that are routinely exchanged in near real-time over the World Meteorological Organization Global Telecommunication System (GTS). A representative distribution of the location of these sites across the Celtic Sea sub-region is shown in Fig. 1(b). In this study, simulations are compared with point observations by considering a mean of model output in the 5 x 5 neighbourhood of grid cells nearest to a given observation site. While this will smooth out some of the very fine resolution detail evident in AMM15 ocean simulations, this is considered a more representative approach than using only the nearest grid cell to reduce the ‘double penalty’ effects common with evaluating high resolution atmosphere or ocean simulations.

5

Around the southern UK coasts, most routine ocean observations are provided by the WaveNet monitoring network (Centre for Environment, Fisheries and Aquaculture Science; Cefas, <http://wavenet.cefas.co.uk>) and the Channel Coast Observatory (<http://www.channelcoast.org>). A number of these in Fig. 1(b) are sites where SST and near-surface wind observations are co-located. Figure 1(b) also highlights how the majority of ocean observing sites are located within only a few kilometres of the coast, and are therefore most representative of near-coastal conditions.

10

This study also uses atmosphere and ocean observations from a number of different sensors co-located at the L4 site of the Western Channel Coast Observatory (WCO; Smyth et al., 2010. See also <https://www.westernchannelobservatory.org.uk>). L4 is located at 50° 15'N, 4° 13'W, about 6 km away from the southern England coast, where the sea is about 50 m deep. A variety of long-term records of physical ocean, atmosphere and marine biogeochemical observations are recorded at L4 (Smyth et al., 2014). Of interest here are the in-situ surface and depth profile temperature measurements from a CTD, air temperature and

15

wind speed measurements, and total and diffuse solar radiation measurements within the 400 – 2700 nm wavelength range using a SPN1 Sunshine Pyranometer.

20

## 3 Results

### 3.1 Domain-wide sea surface temperature (SST)

Figure 2 summarises the mean difference between ocean model SST and in-situ buoy observations across the AMM15 domain (e.g. see Fig. 1(b) of Lewis et al. (2018) for locations) during July 2014. Statistics of the mean difference (MD) and root mean square difference (RMSD) relative to all observations across the month are listed in Table 2. Figure 2 demonstrates that all ocean simulations had the same initial condition, which for this case was on average about 0.8 K warmer than observed. A summer time warm bias relative to OSTIA was noted by Graham et al. (2018). This warm difference is maintained throughout the month for the FOR\_GL simulation, with MD over the month of 0.73 K. This is consistent with the AMM15 run used to provide the initial conditions also being forced with a global-scale meteorology and being a well spun-up ocean state (Graham et al., 2018), so that the bias inherited from the initial condition is maintained. By contrast, the mean difference is substantially

25

30



reduced comparing FOR\_HI to observations (MD = 0.40 K), with FOR\_GL and FOR\_HI results diverging within the first few days of the simulation. This indicates improved SST prediction can be achieved for the NWS when applying the high resolution meteorological forcing.

Further reduction of the SST bias seen in Fig. 2 when considering coupling between the high resolution ocean and atmosphere models in CPL\_AO (MD = 0.26 K). There is some additional value evident from coupling information of the wave state to ocean and atmosphere components in CPL\_AOW (MD = 0.20 K), although this is of secondary importance to the impact of either changing atmosphere resolution or ocean-atmosphere coupling.

### 3.2 SST in the Celtic Sea

To further examine the sensitivity highlighted in Fig. 2, the remaining analysis focuses on results across the Celtic Sea region only, and considers simulation results over the 10-day period between 20 July and 30 July 2014, as being representative of the different ocean simulations having spun up sufficiently from the same initial condition. This is supported by the summary statistics considering only this region and period listed in Table 2, from which broadly consistent conclusions can be drawn as from the statistics obtained for the full domain and simulation duration. In this case, the MD for CPL\_AOW is 1 K smaller than that for FOR\_GL results, and the RMSD is reduced from 1.6 K to 1.0 K.

A snapshot illustration of SST across the Celtic Sea on 28 July 2014 from FOR\_GL and FOR\_HI simulations show qualitatively very consistent patterns (Fig. 3), with areas of cooler water around west-facing peninsulas such as the Ushant front region to the west of Brittany, and around south-western England. Simulated SST across much of the Celtic Sea is relatively cooler in FOR\_HI than FOR\_GL however. Both simulations have warmer surface water in near-coastal regions than observed, such as in the Bristol Channel where the simulated SST exceed 294.5 K. The mean impact of coupling on SST is shown in Fig. 3(c) as an average across the 10 day period. This shows an extensive region where SST is reduced by more than 0.5 K across the Celtic Sea. While differences are lower through the English Channel, stronger relative cooling is also apparent along the coastlines of southern Wales, within the Bristol Channel, and around the Isle of Wight to the east of the domain section. There is qualitatively improved agreement of simulated SST with coastal observations across the region for CPL\_AOW, with relative improvements in RMSD in excess of 20 % at all near-coastal observing sites (Fig. 4).

SST results at L4 between 20 and 30 July 2014 are shown in Fig. 5(a). At this location, the coupled experiments are cooler than observed, although the lowest RMSD (of 0.5 K) is obtained for CPL\_AOW. The SST observations at L4 during late July 2014 were highly variable, with an observed range of 4 K shown in Fig. 5(a). On several days (e.g. 20, 21, 23, 26 and 29 July) a tidally-forced heating signal of about 1 K is apparent. This was particularly strong on 22 and 25 July however, potentially linked to strong solar heating in addition to tidal influence, when a range of 2 K and 3 K were observed respectively. More synoptic-scale influences appear to dominate on 27 and 28 July when the observed SST cycle was relatively diminished. The SST variability of FOR\_GL is in general stronger than observed, but reasonably well captured by all other ocean simulations with high-resolution atmosphere forcing. This is not the case on 25 July however, when the increase in FOR\_GL temperature through the day matches the observed range, while all other simulations fail to replicate such strong temperature variation.



In addition to surface measurements, depth resolved temperature data are routinely taken using CTD sensors at the L4 site on days when data are manually collected. One such profile was observed during the morning of 28 July 2014, and is compared with daily mean simulated temperature profiles at L4 in Fig. 5(b). The observed profile shows a strong temperature gradient between depths of 10 m and 15 m marking the mixed layer depth (MLD), with well mixed water near the surface and stratified water below to the sea bed. There are substantial differences between the simulated profiles in Fig. 5(b). The excessive surface heating in FOR\_GL can be attributed to a much shallower MLD than observed, such that any input solar heating at the surface will heat a smaller volume of water than in reality. In contrast, the near-surface temperature and MLD is in good agreement with observations on this day in the FOR\_HI simulation with high resolution atmospheric forcing. The strength of cooling across the thermocline is considerably less sharp than observed (or in FOR\_GL), although this may be partly an artefact of using a daily mean rather than instantaneous profile and of averaging simulation results across a 5 x 5 neighbourhood of grid cells. Mean temperatures from FOR\_HI are order 1 K warmer than observed between the MLD and a depth of about 35 m. This mean difference is improved when the ocean and atmosphere are coupled (CPL\_AO). An improved temperature profile at L4 below the mixed layer in the fully coupled CPL\_AOW simulation is offset by a cool surface bias, leading to a relatively weaker temperature transition than in CPL\_AO. Further tuning of the CPL\_AOW system may be appropriate, as discussed by Lewis et al. (2018c, *this issue*).

These results demonstrate that SST and temperature profiles through depth are particularly sensitive to atmospheric forcing resolution and to representation of air-sea interactions across the NWS, with fundamental differences in the vertical structure developing between simulations from a common initial condition over a relatively short period of time.

### 3.2 Surface energy budget

The ocean surface boundary condition characterising the energy budget in NEMO is expressed in terms of the solar radiation,  $Q_{SW}$ , that penetrates the top few metres of the ocean, and a non-penetrative component,  $Q_{ns}$ , which only heats or cools the surface (Madec et al., 2016). In the AMM15 configuration,  $Q_{SW}$  specifies the net shortwave radiation at the surface simulated by an atmosphere model across all wavelengths, and  $Q_{ns}$  is computed from the surface energy budget variables as,

$$Q_{ns} = Q_{LW} - \lambda E - H, \quad (1)$$

with  $Q_{LW}$  denoting the net surface longwave radiation,  $\lambda E$  the latent heat due to evaporation and  $H$  the sensible heat flux. In NEMO, the fraction of  $Q_{SW}$  which penetrates to lower depths is controlled by the  $m_{abs}$  parameter. In the simulations considered in this study, it is assumed that 66% of radiation is absorbed at the surface (Lewis et al., 2018b).

The spatial distribution of  $Q_{SW}$ ,  $Q_{LW}$ ,  $\lambda E$  and  $H$  used as forcing for FOR\_GL (i.e. interpolated from the global-scale operational MetUM), FOR\_HI (i.e. interpolated from the variable resolution regional atmosphere simulation) and from CPL\_AO and CPL\_AOW coupled systems are illustrated in Fig. 6. Snapshots of the forcing at 1200 UTC on 28 July 2014 show a typical daytime distribution. The magnitude of net solar short-wave radiation of order  $800 \text{ Wm}^{-2}$  (Fig. 6(a)(e)) clearly dominates the heat budget relative to the net long-wave radiation (of order  $70 \text{ Wm}^{-2}$  away from the surface, Fig. 6(b)(f)) and sensible heat flux (10 to  $20 \text{ Wm}^{-2}$  away from the surface across the Celtic Sea, Fig. 6(c)(g)). The latent heating over the ocean



is also shown to be a relatively important contribution to the surface energy balance, with values up to  $150 \text{ Wm}^{-2}$  simulated (positive values indicating a flux of heat to the atmosphere from evaporation of sea surface water). Comparing the spatial distribution of FOR\_GL and FOR\_HI heat budget terms in Fig. 6 shows generally close agreement on the large-scale, particularly for the sensible and latent heating which are driven by near-surface variability, although the magnitude of latent heating in FOR\_HI is larger than FOR\_GL. The local scale variability of heating is substantially greater in FOR\_HI (e.g. Fig. 6(e)) than FOR\_GL (Fig. 6(a)) however, as might be expected given the contrast in atmosphere model resolutions. An imprint of a pattern of convective cells can be seen in the FOR\_HI forcing, which likely leads to highly variable heating in time.

The spatial distribution of time mean differences between CPL\_AOW and FOR\_HI energy budget terms between 20 and 30 July 2014 are also shown in Fig. 6. The impact of coupling on  $Q_{SW}$  and  $Q_{LW}$  is dominated by random changes in the spatial distribution of convection (Fig. 6(i),(j)). Examination of the simulated cloud fields during this period (not shown) indicate substantial changes in the exact spatial distribution of clouds at any given time between FOR\_HI and CPL\_AOW for example. The clearest impact of air-sea coupling is on the latent heat flux, which is broadly reduced by order 20% across the Celtic Sea in CPL\_AOW. There is also some evidence that the latent heat flux is increased in those near-coastal regions identified as being cooler in CPL\_AOW than FOR\_HI, where the coupled simulation SST was in closer agreement with observations in Fig. 3(c).

The sunshine pyranometer sensor at L4 provides a rare source of observations of the solar radiation over the ocean (Fig. 7(a)). The raw measurements at 1 min sampling frequency have not been corrected for wave motion, which can lead to considerable variability, particularly when the sea state increases. The data shown in Fig. 7(a) are hourly mean values and therefore considered as being representative. The total observed solar radiation exceeds  $800 \text{ Wm}^{-2}$  on several days between 20 and 30 July 2014, particularly on 20 – 23 July, but increased cloud on 24 July leads to the most of the observed radiation coming from the diffuse component at L4. Given that the observations cover the wavelength range 400 – 2700 nm, these are not directly compared with the model data. The time series of simulated  $Q_{SW}$  across all wavelengths at the L4 location (Fig. 7(b)) shows broad agreement however. On most days, the simulated peak in short-wave flux at L4 differ between the sources of atmosphere data considered within  $100 \text{ Wm}^{-2}$  and with FOR\_GL typically lower than the high resolution data. This could be related to the different temporal resolution of the data, and the 3 h updates of FOR\_GL being insufficient to adequately capture the daytime maximum. The warm surface temperature bias of FOR\_GL at L4 appears to result despite rather than because of this difference however. The global-scale and high resolution data are very different on 24 July, when FOR\_GL has much lower  $Q_{SW}$ , in good qualitative agreement with the L4 observations (Fig. 7(a)). The FOR\_HI and coupled simulations all have a strong diurnal variation in contrast on this day. Despite this, the rate of simulated SST change at L4 in Fig. 5(a) on this day was generally consistent across each simulation, suggesting this to be mostly tidally-driven rather than a result of local heating.

Although it is particularly challenging to routinely measure all components of the surface energy budget over the ocean (Yu et al., 2012), the availability of both air and surface temperature observations at L4 enables at least some comparison of the near-surface stability profile (air – surface temperature) against the high-resolution atmosphere simulations (Fig. 7(c)). The magnitude of the observed diurnal variability is in general well captured by all simulations, although air-sea coupling appears



to correct periods on 22, 23 and 29 July when the FOR\_HI regional atmosphere simulation has surface temperature too warm relative to air temperature, which cause spikes in sensible heat flux (not shown).

Taking a broader perspective of the surface energy balance across all sea areas in the Celtic Sea region shows the net effect of the different atmosphere forcing and air-sea coupling (Fig. 8). Here, variables are averaged across all model grid cells over sea  
5 in the region. In contrast to Fig. 7(b) for the L4 site, the accumulated net radiation (sum of short-wave and long-wave) across the whole region in Fig. 8(a) shows more consistently increased net radiation in the FOR\_GL data. On 22 July 2014 for example, the daytime maximum net radiation is over  $150 \text{ W m}^{-2}$  higher in FOR\_GL than the high resolution data. Values are also consistently higher during night time in the global resolution data. These differences are reflected in a mean net radiation flux over the 10 days shown of  $244 \text{ W m}^{-2}$  in FOR\_GL compared with  $227 \text{ W m}^{-2}$  in the CPL\_AOW simulation. The mean net  
10 radiation for the Celtic Sea is order 7% higher in FOR\_GL data than any of the high resolution runs. This difference is consistent with the warm SST bias of FOR\_GL relative to FOR\_HI or coupled ocean simulations being driven by a relatively higher net radiation when using the global-scale atmospheric forcing relative to the regional scale. Figure 6 illustrates the FOR\_GL simulated radiation to be a relatively smooth field while high variability of radiation between convective cells in FOR\_HI and coupled simulations produce patches of relatively reduced heating (Fig. 6(a)). Some evidence of this is apparent  
15 in the time series of net short-wave radiation at L4 on 28 July 2014 in Fig. 7(b). The effect of resolution is also highlighted through considering the standard deviation of net surface radiation across the region (not shown). A summary of these results is given in Table 3, which shows that daytime maximum values in excess of  $250 \text{ W m}^{-2}$  are calculated using either FOR\_HI or coupled results. In contrast, the standard deviation of the FOR\_GL radiation data are consistently lower during both day and night and with a maximum standard deviation of less than  $200 \text{ W m}^{-2}$ , but typically of order 20-50% lower than high resolution  
20 atmosphere simulation values. This provides some evidence that the differences between the representation of the surface energy budget in the global and regional-scale atmosphere simulations is driven mostly by the change in grid resolution and the change from parameterised to explicitly represented convection, rather than from differences between the underpinning MetUM radiation and cloud parameterisation choices, which might be expected to principally drive differences in the mean conditions rather than the spatial variability.

25 Time series of the non-penetrating radiation term,  $Q_{ns}$  (Eq. (1)), at L4 (not shown) also demonstrate much greater variability for the high resolution forcing, and substantial differences between FOR\_HI and the coupled simulations (with CPL\_AO and CPL\_AOW being quite consistent with each other). Considering the accumulated  $Q_{ns}$  across the Celtic Sea (Fig. 8(b)) shows much smaller net differences between experiments than for  $Q_{sw}$ . The difference between global and regional-scale time series on 27 – 29 July can be attributed to the sensitivity to latent heat flux (Fig. 8(c)). The reduced latent heating due to coupling  
30 during this period also results in a less strong upward (i.e. less negative)  $Q_{ns}$  for coupled results relative to FOR\_HI in Fig. 7(b).

In summary, the key sensitivity for ocean forecasting of differences in the surface energy balance from different sources of meteorological forcing is in the representation of the net short-wave radiation. A second-order but non-negligible differences in the latent heat flux is also found. When using a global-scale simulation, as typical for most operational ocean forecast



systems, the high spatial variability associated with convection is not captured, which leads to a larger accumulated heating over a given region in this case. Applying a more spatially variable representation of the surface energy budget when applying using high-resolution forcing (FOR\_HI) or atmosphere-ocean coupled systems (CPL\_AO or CPL\_AOW) led to the improvement to the warm SST bias found in the FOR\_GL ocean simulation.

### 5 3.3 Near-surface wind speed

Snapshots of the global-scale and high-resolution regional atmosphere model wind speed at 10 m above the surface in Fig. 9 also reflect the much finer convective structures simulated in the FOR\_HI simulations (Fig 9(b)). The general structure of wind speed available from the operational global MetUM (Fig. 9(a)) is in qualitative agreement with in-situ observations at this time, particularly in reflecting areas of reduced wind speed across the Bristol Channel and off the southern England coast. The observations over sea are spatially more variable than FOR\_GL across the region however. In contrast, the FOR\_HI data show an area of strong convective activity over the Celtic Sea, and the spatial variability of wind speed over the ocean qualitatively appears to be as high as over land (Fig. 9(b)). The impact of coupling, quantified as the mean difference over the 10-day period between 20 and 30 July 2014, shows wind speed differences of  $\pm 0.5 \text{ ms}^{-1}$ , largely focused in the English Channel rather than Celtic Sea. The contrast between the spatial variability of wind speed between FOR\_GL and FOR\_HI further supports the assessment in Sect. 3.2 that the change in surface energy budget characteristics between the different sources of forcing were driven more by the change in atmosphere grid resolution than by changes to the underpinning model physics. The ocean forcing and coupled results are compared with near-surface wind speed observations at L4 in Fig. 10(a). This shows results typical of that found at other sites in the region (Fig 10(b)) and more generally from analysis of a number of case studies by Lewis et al. (2018a, 2018b) for example. FOR\_GL data follow the day-to-day variability of observed wind speed closely (MD =  $-0.07 \text{ ms}^{-1}$ , RMSD =  $1.29 \text{ ms}^{-1}$ ). By contrast, all high resolution experiments are biased fast (e.g. MD =  $1.4 \text{ ms}^{-1}$  for CPL\_AOW) and with increased RMSD relative to observations. The high temporal variability of wind speed also appears to exceed the observed variability. Figure 11 summarises the mean and range of differences between the global-scale forcing and CPL\_AOW simulations relative to all observations across the Celtic Sea region. The wind speed bias in CPL\_AOW (and other high resolution data, not shown) becomes particularly high on 27 July. The summary metrics indicate that both CPL\_AO and CPL\_AOW simulations have reduced differences to observations than FIX\_HI during the period, although the influence of wave coupling feedbacks is generally small at this time of year. Table 3 summarises the enhanced wind speed variability with increased model resolution in terms of the standard deviation of values across the Celtic Sea region for each simulation. Given the strong sensitivity of surface waves to the near-surface winds, the different characteristics of simulated winds between global and regional-scale systems has been found to have a detrimental impact of the quality of wave model simulations when forced with high-resolution data (Lewis et al., 2018a). As demonstrated in Fig. 10(a), this can be mitigated to some extent through coupling, but it remains challenging to improve the quality of wave forecasts relative to a system with global-scale forcing.



### 3.4 Partially coupled sensitivity experiments

Further work is clearly required to better understand and improve the quality of near-surface winds in the regional atmosphere model. It is therefore of interest to note that the quality of SST from the FOR\_HI and coupled ocean simulations was improved relative to FOR\_GL, perhaps despite the change in wind speed characteristics.

- 5 Two additional ocean-atmosphere coupled simulation experiments have therefore been conducted to further assess the impact of the energy budget and wind speed forcing changes on the ocean simulation. In pCPL\_WIN, only the wind speed components are coupled between the atmosphere and ocean, and radiation variables read from the operational global forcing. In pCPL\_RAD, only the radiation variables are coupled and the global-scale wind speed forcing is used. In both simulations, the exchange of variables from the ocean to the atmosphere was the same as in CPL\_AO.
- 10 The summary results in Fig. 12 shows that SST is improved in pCPL\_RAD (MD = 0.76 K, RMSD = 1.18 K) relative to FOR\_GL, and has similar performance to FOR\_HI. This improvement is not as large as found when coupling both radiation and wind speed in CPL\_AO however, suggesting that ensuring that the ocean state is properly in balance with the atmosphere is also important. Some evidence of the link between SST and near-surface atmosphere conditions within the coupled system was discussed by Lewis et al. (2018b) in considering the relationship between near-surface stability and wind speed over the
- 15 ocean.

- The quality of simulated SST is markedly reduced in pCPL\_WIN (MD = 1.96 K, RMSD = 2.56 K) however, which demonstrates the combined impact of applying a relatively coarse-scale description of the surface radiation budget originating from a global-scale atmosphere, highly variable and biased surface winds originating from a high-resolution regional atmosphere simulation, and the ocean and atmosphere not being in balance through use of the mixed coupling approach with
- 20 incomplete representation of feedbacks. This result also confirms that the improvement in SST found in FOR\_HI relative to FOR\_GL is driven predominantly by the differences to the surface energy budget forcing.

### 4 Conclusions

- This paper has demonstrated that simulation of ocean temperature for the NWS is sensitive to the atmospheric forcing at the surface. Better agreement of simulated SST with observations has been found for a near-coastal environment through use of
- 25 information from a high resolution regional atmosphere simulation rather than using data from a global-scale NWP forecast. A key difference in the insolation in the global and convective scale NWP comes from the explicit representation of convective clouds and their impacts on radiation. In addition to the increased spatial variability from convective scale atmosphere simulations, a mean reduced  $Q_{SW}$  of order 7% across the Celtic Sea region has been found compared to the global-scale forcing. In these simulations, which had a positive SST initial bias, this reduction contributed to improved SST prediction.
- 30 The near-surface winds also differ between the global NWP and high-resolution regional atmospheric simulations both in the mean and their variability. The high-resolution winds compare less well to the limited number of observations over the ocean.



It is therefore concluded that the impact of wind forcing is of second order to the treatment of insolation on the quality of SST results.

The SST bias in near-coastal areas is further reduced using two-way coupling between the ocean and atmosphere and further still by including feedbacks with surface waves. Lewis et al. (2018b) for example demonstrated this to be a general result, and is thought to result from the consistent simulation of the ocean and atmosphere and representation of feedbacks across the surface. SST results were improved relative to observations at a number of near-coastal sites during other times of the year (e.g. Figs. 3 and 4 of Lewis et al., 2018b), noting the impact of wave coupling to be more important during an autumn experiment period than found for the July period considered here.

Given the sensitivity of ocean predictions to the surface forcing and coupling demonstrated here it is clear that more routine observations of the components of the surface energy and momentum budgets over the ocean would be of considerable value. In particular, co-location of complimentary measurements of the ocean and atmospheric boundary layers should better enable a more complete representation of surface feedbacks, in order to evaluate and improve prediction systems. Given these are challenging environments for making observations, making more use of the scarce sources of information currently available to the meteorological and oceanographic research communities should also be encouraged as a component of regional model development across both disciplines. The use of fully coupled prediction systems for research provides a framework in which to focus efforts on evaluating the interactions across the ocean surface, and to identify gaps in the current observational capability above and below the surface.

### Acknowledgements

This work originated from initial studies and technical developments conducted under the Copernicus Marine Environment Monitoring Service (CMEMS) evolution project on Ocean-Wave-Atmosphere Interactions in Regional Seas (OWAIRS). CMEMS is implemented by Mercator Ocean in the framework of a delegation agreement with the European Union.

The Western Channel Observatory is funded by the UK Natural Environment Research Council through its National Capability Long-term Single Centre Science Programme, Climate Linked Atlantic Sector Science (grant number NE/R015953/1).



## References

- Banta, R.M., Pichugina, Y.L., Brewer, W.A., James, E.P., Olson, J.B., Benjamin, S.G., Carley, J.R., Bianco, L., Djalalova, I.V., Wilczak, J.M., Hardesty, R.M., Cline, J., and Marquis, M.C.: Evaluating and Improving NWP Forecast Models for the Future: How the Needs of Offshore Wind Energy Can Point the Way. *Bull. Amer. Meteor. Soc.*, 99, 1155–1176, doi:10.1175/BAMS-D-16-0310.1, 2018.
- 5 Bricheno, L.M., Soret, A., Wolf, J., Jorba, O., and Baldasano, J.M.: Effect of High-Resolution Meteorological Forcing on Nearshore Wave and Current Model Performance, *J. Atmos. Oceanic Technol.*, 30, 1021–1037, doi:10.1175/JTECH-D-12-00087.1, 2013.
- Bruneau, N., and Toumi, R.: A fully-coupled atmosphere-ocean-wave model of the Caspian Sea, *Ocean Modelling*, 107, 97–111, doi:10.1016/j.ocemod.2016.10.006, 2016.
- 10 Bush, M., Allen, T., Boutle, I., Edwards, J., Finnenkoetter, A., Franklin, C., Hanley, K., Lean, H., Lock, A., Manners, J., Mittermaier, M., Morcrette, C., North, R., Petch, J., Short, C., Vosper, S., Walters, D., Webster, S., Weeks, M., Wilkinson, J., Wood, N., and Zerroukat, M.: The Met Office Unified Model Regional Atmosphere 1 and JULES Regional Land 1 configurations, *Geosci. Model Dev.*, in preparation, 2018.
- 15 Carniel, S., Benetazzo, A., Bonaldo, D., Falcieri, F.M., Miglietta, M.M., Ricchi, A., and Sclavo, M.: Scratching beneath the surface while coupling atmosphere, ocean and waves: Analysis of a dense water formation event, *Ocean Modelling*, 101, 101–112, doi:10.1016/j.ocemod.2016.03.007, 2016.
- Cavaleri, L.: Wave Modeling—Missing the Peaks. *J. Phys. Oceanogr.*, 39, 2757–2778, doi:10.1175/2009JPO4067.1, 2009.
- 20 Cavaleri, L., Abdalla, S., Benetazzo, A., Bertotti, L., Bidlot, J.-R., Breivik, Ø., Carniel, S., Jensen, R.E., Portilla-Yandun, J., Rogers, W.E., Roland, A., Sanchez-Arcilla, A., Smith, J.M., Staneva, J., Toledo, Y., van Vledder, G.Ph., and van der Westhuysen, A.J.: Wave modelling in coastal and inner seas. *Progress in Oceanogr.*, doi:10.1016/j.pocean.2018.03.010, 2018.
- Clark, P., Roberts, N., Lean, H., Ballard, S. P. and Charlton-Perez, C.: Convection-permitting models: a step-change in rainfall forecasting. *Met. Apps*, 23: 165-181. doi:10.1002/met.1538, 2016.
- 25 Drechsel, S., Mayr, G.J., Messner, J.W., and Stauffer, R.: Wind Speeds at Heights Crucial for Wind Energy: Measurements and Verification of Forecasts. *J. Appl. Meteor. Climatol.*, 51, 1602–1617, doi:10.1175/JAMC-D-11-0247.1, 2012.
- Graham, J. A., O’Dea, E., Holt, J., Polton, J., Hewitt, H. T., Furner, R., Guihou, K., Brereton, A., Arnold, A., Wakelin, S., Castillo Sanchez, J. M., and Mayorga Adame, C. G.: AMM15: a new high-resolution NEMO configuration for operational simulation of the European north-west shelf, *Geosci. Model Dev.*, 11, 681–696, <https://doi.org/10.5194/gmd-11-681-2018>, 30 2018.
- Gronholz, A., Gräwe, U., Paul, A., and Schulz, M.: Investigating the effects of a summer storm on the North Sea stratification using a regional coupled ocean-atmosphere model. *Ocean Dynamics*, 67, 211–235. doi:10.1007/s10236-016-1023-2, 2017.



- Holt, J., Hyder, P., Ashworth, M., Harle, J., Hewitt, H. T., Liu, H., New, A. L., Pickles, S., Porter, A., Popova, E., Allen, J. I., Siddorn, J., and Wood, R.: Prospects for improving the representation of coastal and shelf seas in global ocean models, *Geosci. Model Dev.*, 10, 499-523, doi:10.5194/gmd-10-499-2017, 2017.
- Lebeaupin Brossier, C., Béranger, K., Deltel, C., and Drobinski, P.: The Mediterranean response to different space–time resolution atmospheric forcings using perpetual mode sensitivity simulations, *Ocean Modelling*, 36, 1-25, doi:10.1016/j.ocemod.2010.10.008, 2011.
- Lellouche, J.-M., Greiner, E., Le Galloudec, O., Garric, G., Regnier, C., Drevillon, M., Benkiran, M., Testut, C.-E., Bourdalle-Badie, R., Gasparin, F., Hernandez, O., Levier, B., Drillet, Y., Remy, E., and Le Traon, P.-Y.: Recent updates to the Copernicus Marine Service global ocean monitoring and forecasting real-time 1/12° high-resolution system, *Ocean Sci.*, 14, 1093-1126, doi:10.5194/os-14-1093-2018, 2018.
- Lewis, H. W., Castillo Sanchez, J. M., Graham, J., Saulter, A., Bornemann, J., Arnold, A., Fallmann, J., Harris, C., Pearson, D., Ramsdale, S., Martínez-de la Torre, A., Bricheno, L., Blyth, E., Bell, V., Davies, H., Marthews, T., O'Neill, C., Rumbold, H., O'Dea, E., Brereton, A., Guihou, K., Hines, A., Butenschon, M., Dadson, S. J., Palmer, T., Holt, J., Reynard, N., Best, M., Edwards, J., and Siddorn, J.: The UKC2 regional coupled environmental prediction system, *Geosci. Model Dev.*, 11, 1-42, <https://doi.org/10.5194/gmd-11-1-2018>, 2018a.
- Lewis, H. W., Castillo Sanchez, J. M., Arnold, A., Fallmann, J., Saulter, A., Graham, J., Bush, M., Siddorn, J., Palmer, T., Lock, A., Edwards, J., Bricheno, L., Martínez de la Torre, A., and Clark, J.: The UKC3 regional coupled environmental prediction system, *Geosci. Model Dev. Discuss.*, doi:10.5194/gmd-2018-245, in review, 2018b.
- Lewis, H.W., Castillo Sanchez, J.M., Siddorn, J., King, R.R., Tonani, M., Saulter, A., Sykes, P., Pequignet, A.-C., Weedon, G.P., Palmer, T., Staneva, J., and Bricheno, L.: Can wave coupling improve operational regional ocean forecasts for the North-West European Shelf?, *Ocean Science*, submitted, 2018c.
- Licer, M., Smerkol1, P., Fettich, A., Ravdas, M., Papapostolou A., Mantziafou, A., Strajnar, B., Cedilnik, J., Jeromel, M., Jerman, J., Petan, S., Malaci, V., and Sofianos, S.: Modeling the ocean and atmosphere during an extreme bora event in northern Adriatic using one-way and two-way atmosphere-ocean coupling, *Ocean Science*, 12, 72-86, doi:10.5194/os-12-71-2016, 2016.
- MacLachlan, C., Arribas, A., Peterson, D., Maidens, A., Fereday, D., Scaife, A. A., Gordon, M., Vellinga, M., Williams, A., Comer, R. E., Camp, J., Xavier, P., and Madec, G.: Global Seasonal forecast system version 5 (GloSea5): a high resolution seasonal forecast system, *Q. J. Roy. Meteor. Soc.*, 141, 1072-1084, doi:10.1002/qj.2396, 2015.
- Madec, G., and the NEMO team: “NEMO reference manual 3\_6\_STABLE : NEMO ocean engine”. Note du Pôle de modélisation, Institut Pierre-Simon Laplace (IPSL), France, No 27 ISSN No 1288-1619, 2016.
- Pullen, J., Allard, R., Seo, H., Miller, A. J., Chen, S., Pezzi, L. P., Smith, T., Chu, P., Alves, J., and Caldeira, R.: Coupled ocean-atmosphere forecasting at short and medium time scales, *Journal of Marine Research*, 75, 877-921, doi:10.1357/002224017823523991, 2017.



- Schaeffer, A., Garreau, P., Molcard, A., Fraunié P., and Seity, Y.: Influence of high-resolution wind forcing on hydrodynamic modeling of the Gulf of Lions, *Ocean Dynamics*, 61, 1823–1844 doi:10.1007/s10236-011-0442-3, 2011.
- Smith, R. N. B.: A scheme for predicting layer cloud and their water content in a general circulation model, *Q. J. R. Meteorol. Soc.*, 116, 435–460, <https://doi.org/10.1002/qj.49711649210>, 1990.
- 5 Smyth, T.J., Allen, J.I., Atkinson, A., Bruun, J.T., Harmer, R.A., Pingree, R.D., Widdicombe, C.E., Somerfield P.J.: Ocean net heat flux influences seasonal to interannual patterns of plankton abundance, *PLOS ONE* 9, e98709, doi:10.1371/journal.pone.0098709, 2014.
- Smyth, T.J., Fishwick, J.R., AL-Moosawi, L., Cummings, D.G., Harris, C., Kitidis, V., Rees, A., Martinez-Vicente, V., and Woodward, E.M.S.: A broad spatio-temporal view of the Western English Channel observatory, *Journal of Plankton*
- 10 *Research*, 32, 585–601, doi:10.1093/plankt/fbp128, 2009.
- Tang, Y., Lean, H.W. and Bornemann, J.: The benefits of the Met Office variable resolution NWP model for forecasting convection, *Meteorol. Appl.*, 20, 417-426, doi:10.1002/met.1300, 2013.
- Tolman, H.L.: User manual and system documentation of WAVEWATCH III® version 4.18. NOAA / NWS / NCEP / MMAB Technical Note 316, 282 pp + Appendices, 2014.
- 15 Tonani, M., Sykes, P., King, R.R., McConnell, N., Pequignet, A.-C., O’Dea, E., Graham, J.A., Polton, J., and Siddorn, J.: The impact of a new high-resolution ocean model on the Met Office North-West European Shelf forecasting system, *Ocean Science*, in preparation, 2018.
- Wada, A., Kanada, S., and Yamada, H.: Effect of air-sea environmental conditions and interfacial processes on extremely intense Typhoon Haiyan (2013). *Journal of Geophysical Research: Atmospheres*, 123, 10,379–10,405.
- 20 doi:10.1029/2017JD028139, 2013.
- Wahle, K., Staneva, J., Koch, W., Fenoglio-Marc, L., Ho-Hagemann, H. T. M., and Stanev, E. V.: An atmosphere–wave regional coupled model: improving predictions of wave heights and surface winds in the southern North Sea, *Ocean Sci.*, 13, 289-301, <https://doi.org/10.5194/os-13-289-2017>, 2017.
- Walters, D., Boutle, I., Brooks, M., Melvin, T., Stratton, R., Vosper, S., Wells, H., Williams, K., Wood, N., Allen, T., Bushell,
- 25 A., Copley, D., Earnshaw, P., Edwards, J., Gross, M., Hardiman, S., Harris, C., Heming, J., Klingaman, N., Levine, R., Manners, J., Martin, G., Milton, S., Mittermaier, M., Morcrette, C., Riddick, T., Roberts, M., Sanchez, C., Selwood, P., Stirling, A., Smith, C., Suri, D., Tennant, W., Vidale, P. L., Wilkinson, J., Willett, M., Woolnough, S., and Xavier, P.: The Met Office Unified Model Global Atmosphere 6.0/6.1 and JULES Global Land 6.0/6.1 configurations, *Geosci. Model Dev.*, 10, 1487-1520, <https://doi.org/10.5194/gmd-10-1487-2017>, 2017a.
- 30 Walters, D., Baran, A., Boutle, I., Brooks, M., Earnshaw, P., Edwards, J., Furtado, K., Hill, P., Lock, A., Manners, J., Morcrette, C., Mulcahy, J., Sanchez, C., Smith, C., Stratton, R., Tennant, W., Tomassini, L., Van Weverberg, K., Vosper, S., Willett, M., Browse, J., Bushell, A., Dalvi, M., Essery, R., Gedney, N., Hardiman, S., Johnson, B., Johnson, C., Jones, A., Mann, G., Milton, S., Rumbold, H., Sellar, A., Ujiie, M., Whittall, M., Williams, K., and Zerroukat, M.: The Met Office Unified Model



Global Atmosphere 7.0/7.1 and JULES Global Land 7.0 configurations, Geosci. Model Dev. Discuss., <https://doi.org/10.5194/gmd-2017-291>, in review, 2017b.

Wilson, D. R., Bushell, A. C., Kerr-Munslow, A. M., Price, J. D., and Morcrette, C. J.: PC2: A prognostic cloud fraction and condensation scheme. I: Scheme description, Q. J. R. Meteorol. Soc., 134, 2093–2107, <https://doi.org/10.1002/qj.333>, 2008.

5 Wu, R., Zhang, H., Chen, D., Li, C., and Lin, J.: Impact of Typhoon Kalmaegi (2014) on the South China Sea: Simulations using a fully coupled atmosphere-ocean-wave model, Ocean Modelling, 131, 132-151, doi:10.1016/j.ocemod.2018.08.004, 2018.

10 Yu, L., Haines, K., Bourassa, M., Cronin, M., Gulev, S., Josey, S., Kato, S., Kumar, A., Lee, T., and Roemmich, D.: Towards achieving global closure of ocean heat and freshwater budgets: Recommendations for advancing research in air-sea fluxes through collaborative activities. In Report of the CLIVAR/GSOP/WHOI Workshop on Ocean Syntheses and Surface Flux Evaluation, Woods Hole, Massachusetts, 27-30 November 2012, WCRP Informal/Series Rep. No. 13/2013, ICPO Informal Rep. 189/13, 42 pp., 2013.

15

20



Run ID	Model system <sup>(1)</sup>	Atm. coupled?	Wave coupled?	Information on meteorological forcing / coupling of ocean			
				Source	Grid resolution	MetUM config.	Frequency
FOR_GL	UKO3g	No	No	Global-scale MetUM NWP forecast	Approx. 17 km	GA6.1, GL6.1 (Walters et al., 2017)	Radiation: 180 min Winds: 60 min
FOR_HI	UKO3h	No	No	Regional uncoupled MetUM	Variable resolution, up to 1.5 km	RA1 (Bush et al., 2018)	All: 60 min
CPL_AO	UKC3ao	Yes	No	Regional coupled MetUM			
CPL_AOW	UKC3aow	Yes	Yes	Regional coupled MetUM			

Table 1: Summary of ocean simulation experiments using forced mode and coupled systems. <sup>(1)</sup> The model system names refer to model configurations documented by Lewis et al. (2018b).

Experiment	Full domain, 30 June – 30 July 2014		Celtic Sea region, 20 – 30 July 2014	
	MD (K)	RMSD (K)	MD (K)	RMSD (K)
FIX_GL	0.73	1.41	1.22	1.56
FIX_HI	0.40	1.27	0.63	1.17
CPL_AO	0.26	1.21	0.36	0.99
CPL_AOW	0.20	1.24	0.22	0.99

5 Table 2: Summary of mean difference of SST (Model – Observation) and root mean square difference (RMSD) comparing each simulation experiment with observations. Statistics computed using observations across the full AMM15 domain through July 2014 and those using only observations in the Celtic Sea region (Fig. 1(b)) during the last 10 days of July 2014 are listed.

Experiment	Net radiation, standard deviation ( $W m^{-2}$ )			10 m wind speed, standard deviation ( $m s^{-1}$ )		
	Mean	Max	Min	Mean	Max	Min
FIX_GL	55	190	10	1.33	1.88	0.82
FIX_HI	78	277	16	1.57	2.13	1.15
CPL_AO	81	268	17	1.56	2.23	1.08
CPL_AOW	79	274	15	1.54	2.14	1.11

10 Table 3: Summary of mean, maximum and minimum values of the spatial standard deviation of net radiation and 10 m wind speed computed across the Celtic Sea between 20 and 30 July 2014 for each experiment.

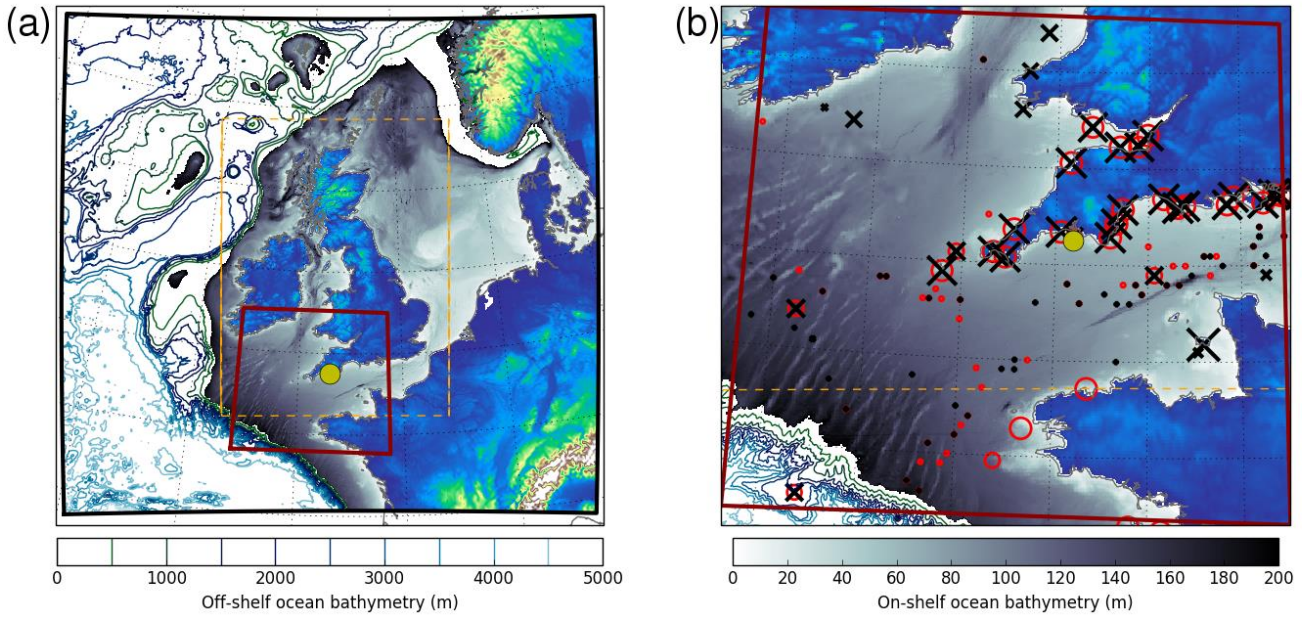


Figure 1: (a) Regional ocean model bathymetry for the NWS system. The colour scale is valid for locations off the shallow shelf region. Also shown are the Celtic Sea study area (red box) and location of the L4 ocean buoy (yellow circle). The dashed orange area marks the inner region of the UKV atmosphere grid. (b) Zoom in of ocean model bathymetry across the red box region (note on-shelf colour scale) Also shown are potential locations of in-situ observations of wind (black cross) and SST (red circle) available for evaluation on 20 July 2014. The L4 ocean buoy is also shown (yellow circle).

5

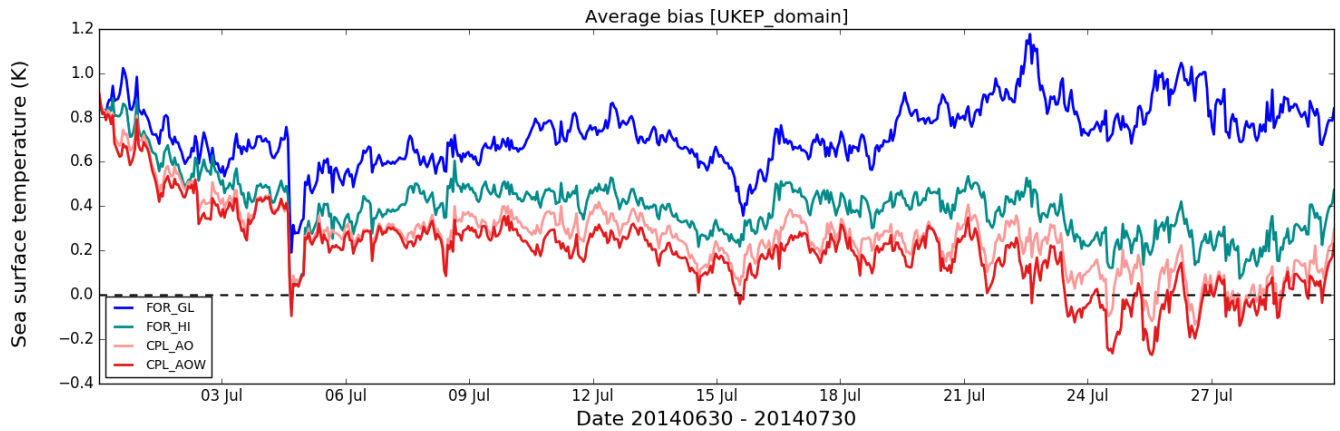
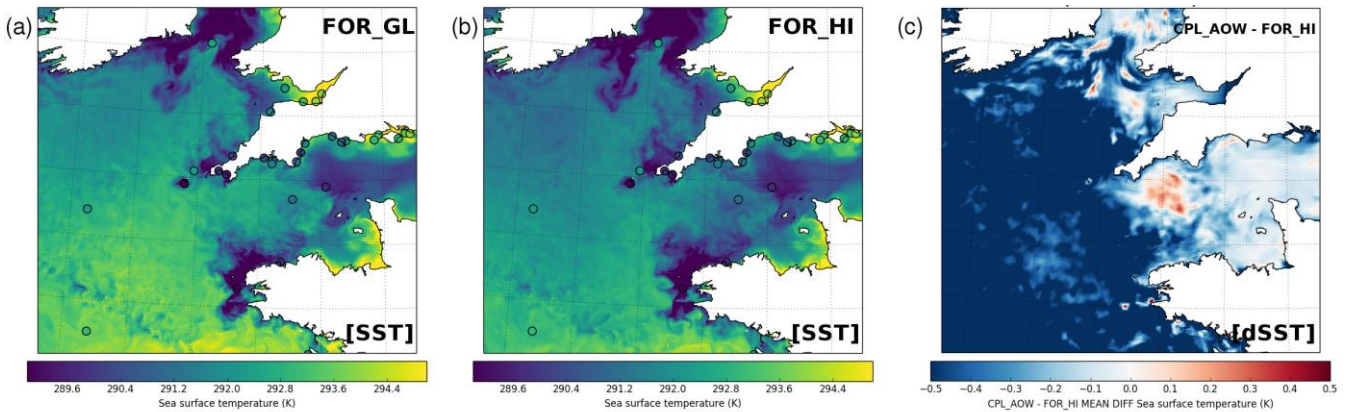
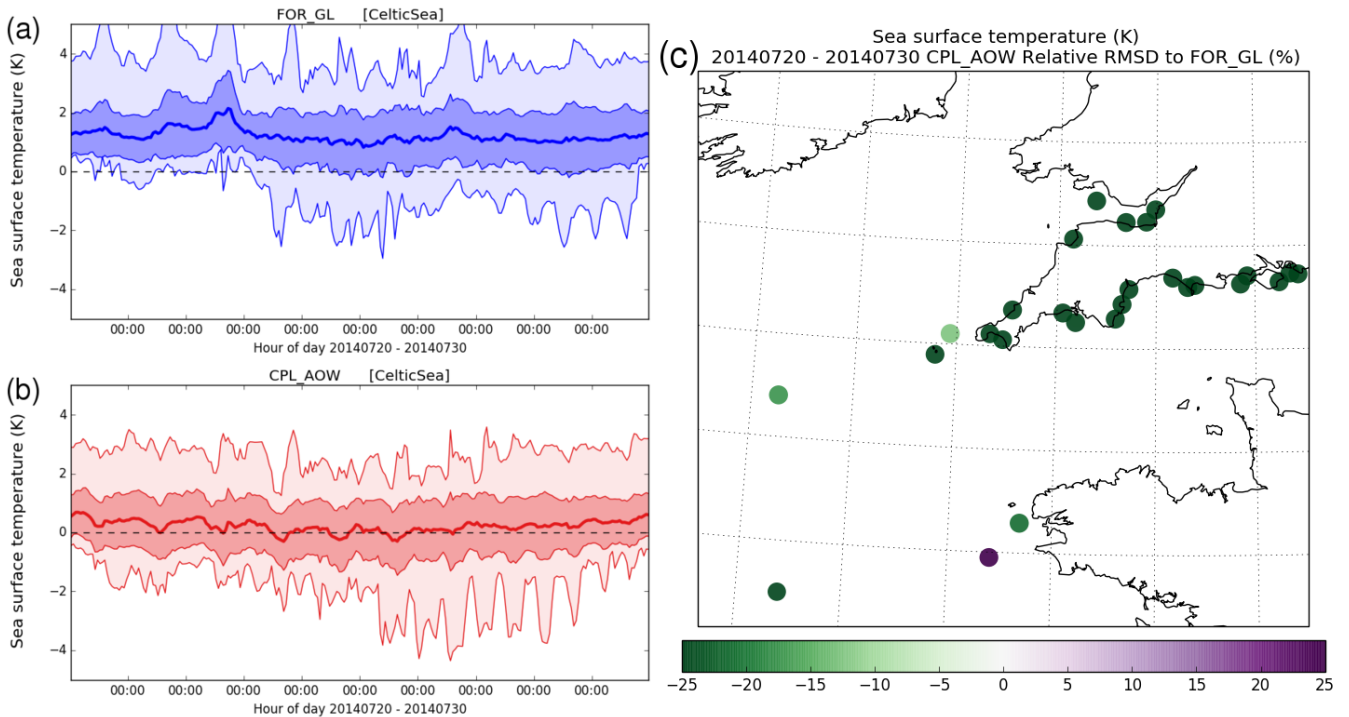


Figure 2: Evolution of mean bias (Model – Observation difference) in SST for each experiment during July 2014 relative to all in-situ observations across the AMM15 model domain.

10



5 **Figure 3:** Snapshot illustration of ocean model SST across Celtic Sea region valid at 1200 on 28 July 2014 from (a) FOR\_GL configuration using global NWP forcing and (b) FOR\_HI using 1.5 km resolution atmospheric forcing. Shaded circles show the distribution of instantaneous observed SST. (c) Mean impact of model coupling on SST over 10 day period between 20 and 30 July 2014, comparing CPL\_AOW with FOR\_HI.



10 **Figure 4:** Evolution of SST bias (model – observation) across Celtic Sea between 20 and 30 July 2014 for (a) FOR\_GL and (b) CPL\_AOW configurations relative to in-situ observations. The mean bias across all sites is shown as a thick line, bounded by +/- 1 standard deviation (darker shading) and maximum/minimum differences (lighter shading). (c) Percentage change in RMSD relative to in-situ observations for CPL\_AOW results relative to FOR\_GL over this period.

15

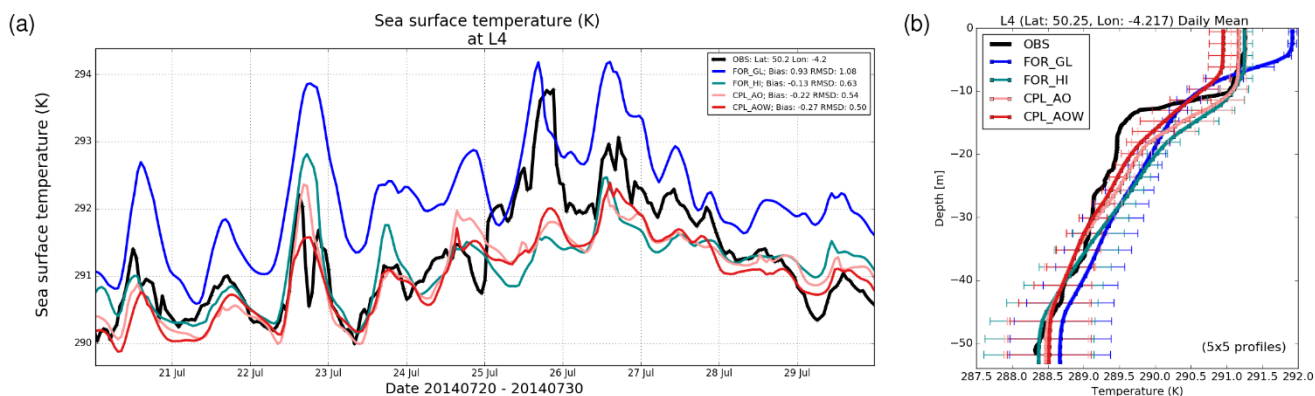
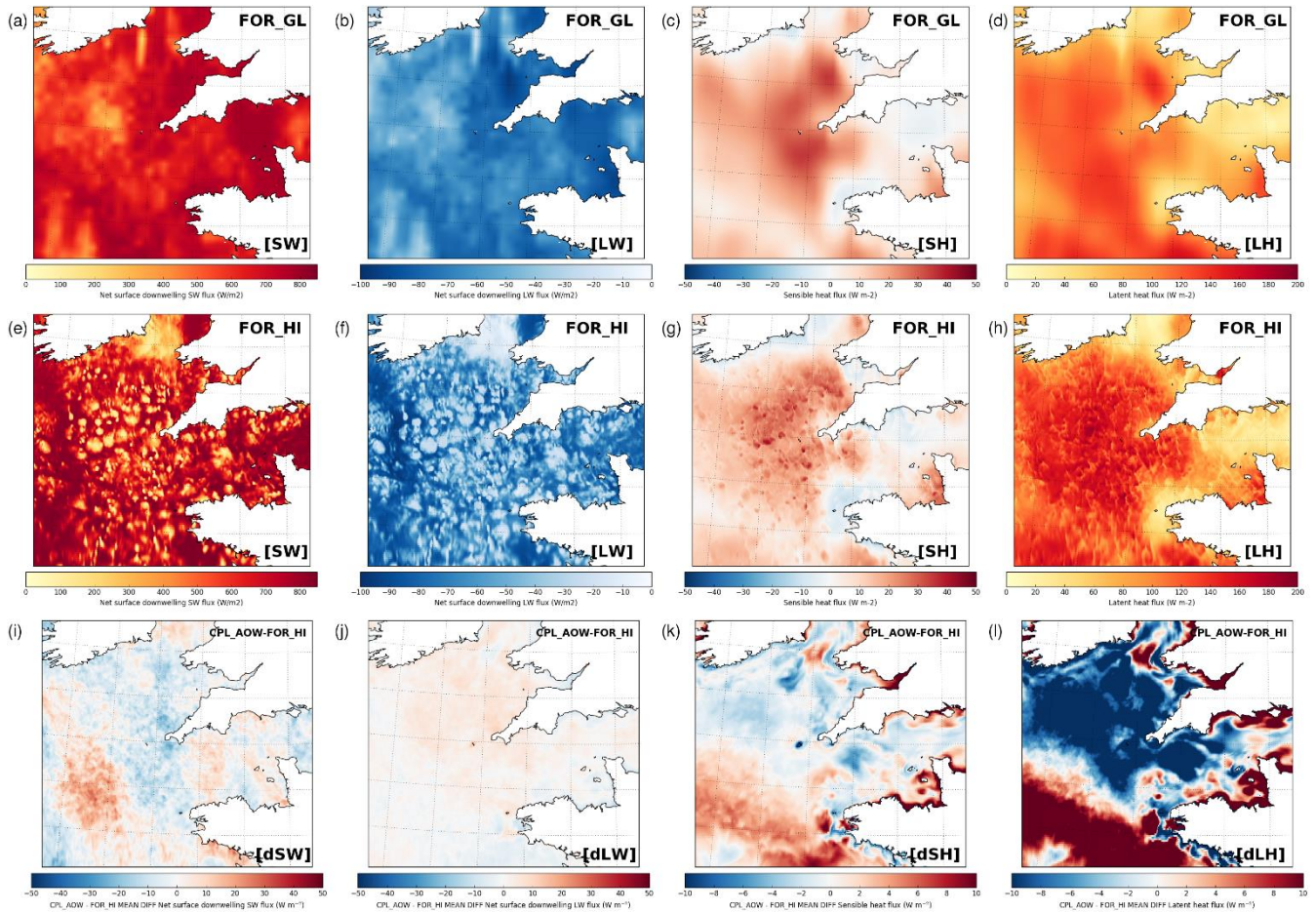


Figure 5: (a) Time series of simulated and observed SST at the L4 ocean buoy (Fig. 1) between 20 and 30 July 2014. Model series are shown as a mean from a 5 x 5 set of model grid cells nearest the observing site. (b) Vertical temperature profile observed by CDT at the L4 location on 28 July 2014 and daily mean profiles for each simulation experiment on that date. Error bars indicate 1 standard deviation around the spatial mean profile.

5

10



**Figure 6:** Snapshot illustration of surface energy balance terms used in (a-d) FOR\_GL and (e-h) FOR\_HI atmospheric forcing, valid for 1200 on 28 July 2014. The impact of model coupling is shown in (i-l) as the difference between 10-day averaged CPL\_AOW and FOR\_HI results across all times of day. Variables considered are (a,e,i) net surface downwelling shortwave flux, (b,f,j) net surface downwelling longwave flux, (c,g,k) sensible heat flux and (d,h,l) latent heat flux.

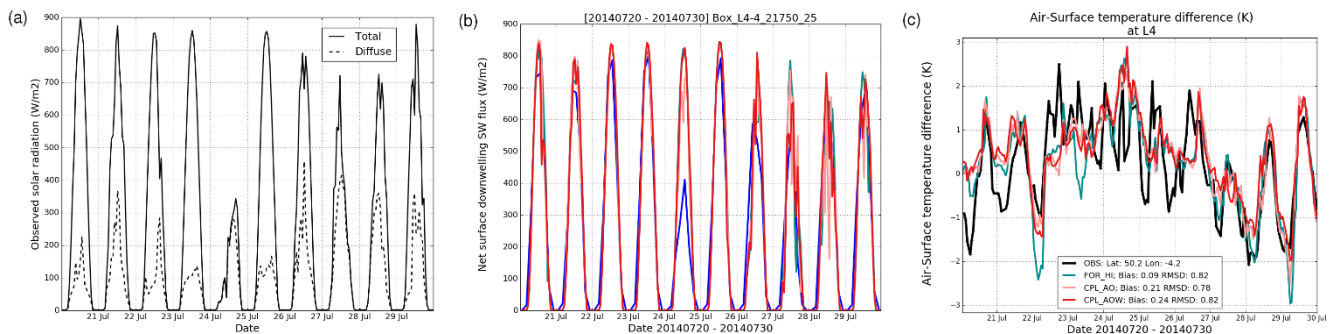


**Figure 7:** (a) Hourly mean observations of total and diffuse solar irradiance components at the L4 buoy between 20 and 30 July 2014. Time series of simulated (b) net surface downwelling shortwave flux and (c) observations and simulations of near-surface temperature difference ( $T_{\text{air}(1.5 \text{ m})} - \text{SST}$ ).

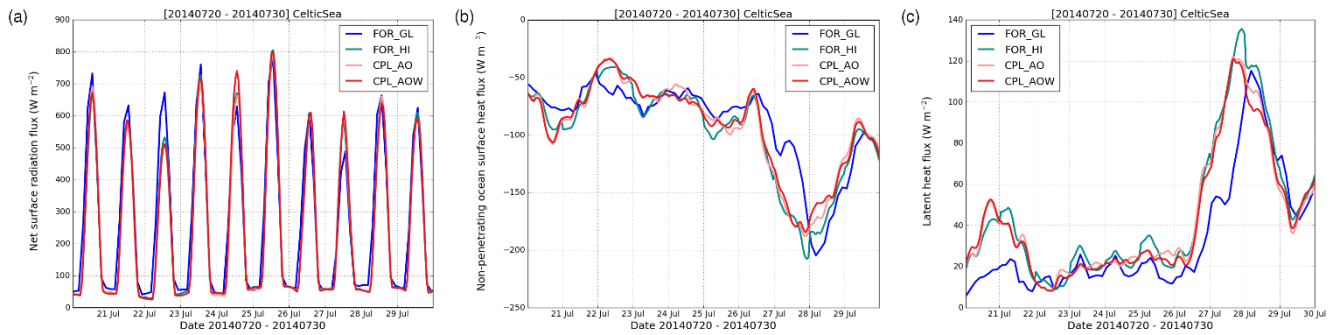


**Figure 8:** Time series of mean simulated surface energy balance variables across sea areas in the Celtic Sea region (Fig. 1(b)), for (a) net surface radiation [net short-wave + net long-wave], (b) non-penetrating ocean heat flux [Eq. (1)] and (c) latent heat flux.

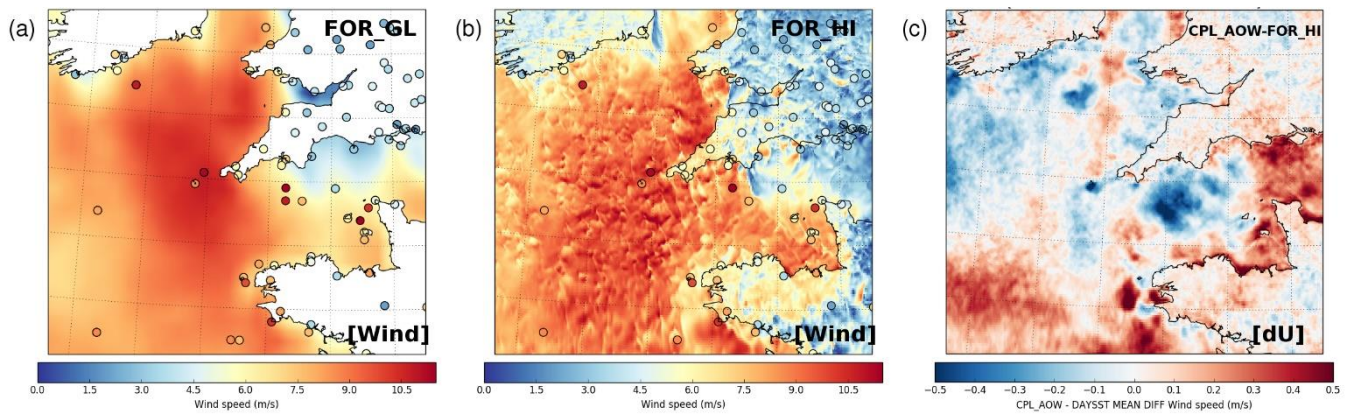


**Figure 9:** Snapshot illustration of near-surface wind speed forcing across Celtic Sea region valid at 1200 on 28 July 2014 used for (a) FOR\_GL configuration (global-scale NWP) and (b) FOR\_HI (1.5 km resolution atmosphere model). Shaded circles show the distribution of instantaneous observed wind speed. (c) Mean impact of model coupling on near-surface wind speed over 10 day period between 20 and 30 July 2014, comparing CPL\_AOW with FOR\_HI.

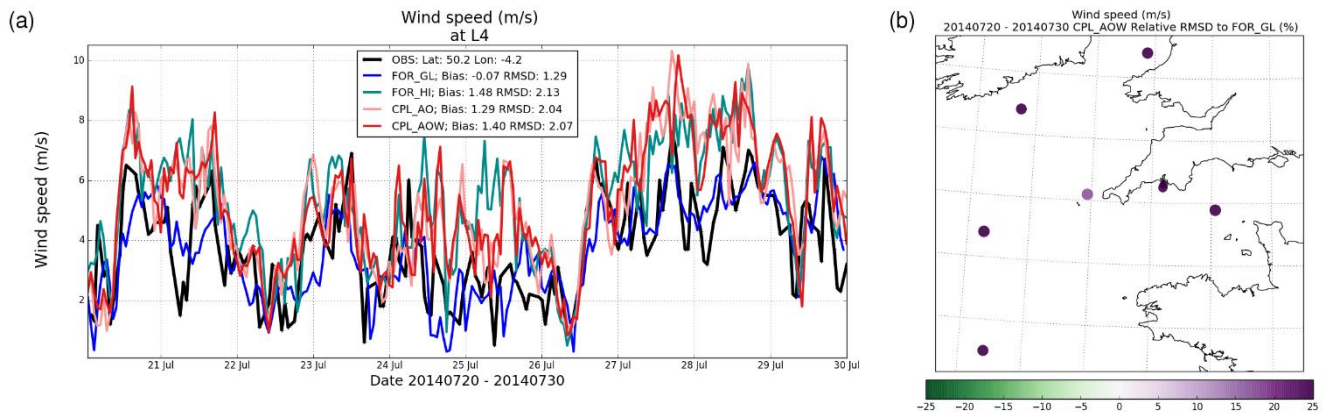


**Figure 10:** (a) Time series of simulated and observed near-surface wind speed at the L4 ocean buoy between 20 and 30 July 2014. Model series are shown as a mean from a 5 x 5 set of model grid cells nearest the observing site. (b) Percentage change in RMSD relative to in-situ observations for CPL\_AOW wind speeds relative to FOR\_GL forcing over this period.

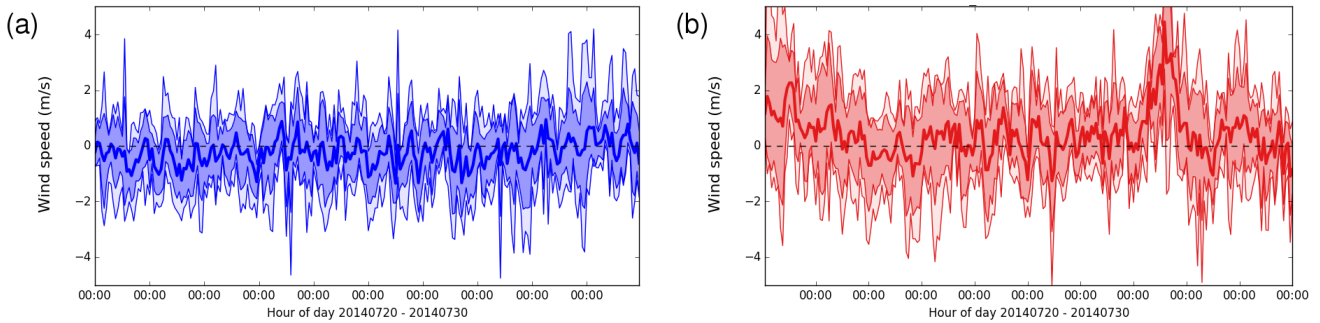


**Figure 11: Evolution of near-surface wind speed bias (model – observation) across Celtic Sea between 20 and 30 July 2014 for (a) FOR\_GL forcing and (b) CPL\_AOW simulation relative to in-situ observations. The mean bias across all sites is shown as a thick line, bounded by +/- 1 standard deviation (darker shading) and maximum/minimum differences (lighter shading).**

5

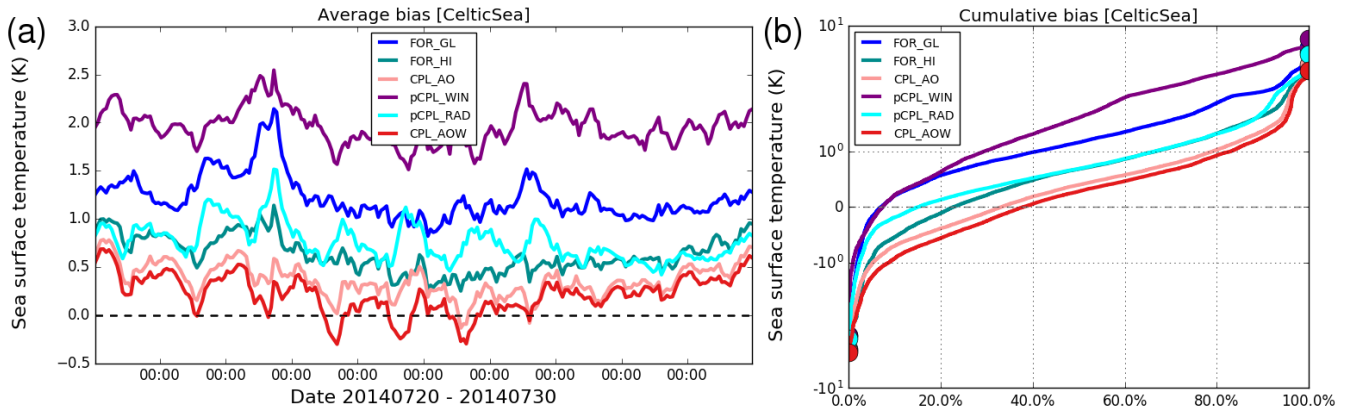


**Figure 12: (a) Evolution of bias (model – observations) in SST for all ocean forced, coupled and partially coupled experiments between 20 and 20 July 2014 relative to all in-situ observations across the Celtic Sea study area (red box in Fig. 1). (b) Cumulative SST bias distribution for each experiment.**